2002 IEEE Int'l Symp. on Circuits and Systems (ISCAS 2002)
Scottsdale AZ, USA, May 26–29, 2002

SPACE-TIME VECTOR DELTA-SIGMA MODULATION

Dan P. Scholnik scholnik@nrl.navy.mil
Jeffrey O. Coleman jeffc@alum.mit.edu
Naval Research Laboratory, Washington, DC

ABSTRACT

Classical delta-sigma modulation gains resolution through temporal oversampling by using a high-speed, low-resolution quantizer and shaping the resulting quantization errors out of the signal band. Likewise, spatial delta-sigma modulation is often used in image halftoning to create high-visual-quality binary images. We consider combining spatial and temporal delta-sigma modulation to reduce temporal oversampling requirements in high-SNR antenna transmit arrays using simple high-power switches as the output amplifiers. We introduce a vector delta-sigma architecture that allows noise shaping jointly in both temporal and spatial frequency. The two-dimensional pseudo-shift-invariant delta-sigma architecture commonly used for image halftoning is realized as a special case, and we consider when such a simplified model may be appropriate.

1. INTRODUCTION

Delta-sigma ($\Delta\Sigma$) modulation is widely used in D/A and A/D conversion to obtain high precision, linearity, and dynamic range in exchange for a higher sampling rate or lower bandwidth [1] by placing a low-resolution quantizer inside a feedback loop to spectrally shape quantization noise to minimize its interference with the signal. Out-of-band quantization noise is then removed with digital or analog filtering according to the application (A/D or D/A). High oversampling rates (rates relative to signal bandwidths) result in signal-to-noise ratio (SNR) levels often exceeding the roughly 100 dB limit of conventional (Nyquist-rate) converters. One-bit quantizers have traditionally been used for their automatically near-ideal characteristics, but newer multi-bit $\Delta\Sigma$-like architectures [2, 3, 4] based on dynamic element matching (DEM) spectrally shape hardware-mismatch errors as well and lower oversampling requirements by increasing parallelism.

Spatial multidimensional $\Delta\Sigma$ modulation of images to produce halftone images from continuous-tone ones is known as *error diffusion* [5, 6]. Typically, continuous-valued image files viewed on a monitor at 100 dots per inch (DPI) are converted to 600+ DPI binary-valued images for printing. Single-bit quantizers are used, but less for being ideal than because they model printers and displays with binary-valued pixels. The inherent lowpass nature of human vision then replaces the explicit post-modulator filtering that removes quantization noise in temporal $\Delta\Sigma$ modulation.

Given the benefits of temporal and spatial $\Delta\Sigma$ modulators individually, it is natural to consider jointly oversampling space and time in a space-time $\Delta\Sigma$ modulator. Although application to halftoned movies has been briefly considered [7], the primary application of interest here is to digitally controlled transmit arrays of medium to high bandwidth for RF systems in which hardware simplicity and near-perfect amplifier linearity make single-bit outputs attractive. A new class of high-speed, high-power RF switches have been proposed [8] for this application. The same basic principles also apply to acoustic arrays. We present a vector space-time $\Delta\Sigma$ modulation architecture that jointly shapes the quantization noise in both temporal and spatial frequency. By oversampling spatially and exploiting the bandpass nature of wave propagation, temporal oversampling requirements can be reduced. Unlike other multidimensional $\Delta\Sigma$ architectures [6, 9] neither spatial shift-invariance nor uniform spatial sampling is assumed. We show that the existing structures can be realized as a special case of the proposed architecture, and consider when a shift-invariant model provides a good approximation.

This work was supported by the Office of Naval Research.

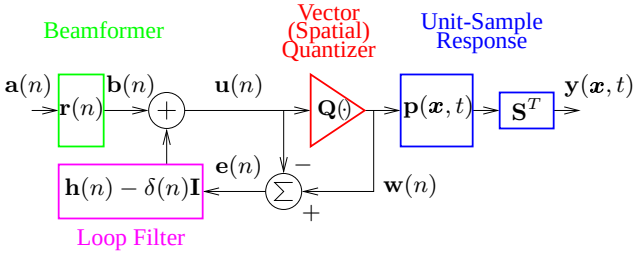

Figure 1: Space-time $\Delta\Sigma$ modulator feeding an antenna array.

2. SYSTEM ANALYSIS

The proposed architecture for space-time $\Delta\Sigma$ modulation is shown in Fig. 1 and is a natural extension of an earlier vector $\Delta\Sigma$ architecture [10]. The $N \times 1$ input vector $\mathbf{a}(n)$ contains the scalar waveforms to be transmitted, while the columns of $K \times N$ matrix $\mathbf{r}(n)$ act as individual beamformers to generate K individual array-element drives. Each vector coordinate inside the $\Delta\Sigma$ loop corresponds to a hardware *unit element*, perhaps a high-power switch feeding a radiator in the array. We thus associate coordinate k with the spatial location $\mathbf{x}_k$ of the physical element. The loop is closed around the loop filter operating on the quantization error of the vector (spatial) quantizer. The quantizer output is then the $\Delta\Sigma$-modulated space-time signal fed to the array. The physical radiators are modeled by the $L \times 1$ block-matrix unit-sample response $\mathbf{p}(\boldsymbol{x},t)$, where L is the number of polarization components of interest. Each block is a $K \times K$ matrix, where the diagonal elements represent the current-density response of the corresponding radiator to its own input, and the off-diagonal terms represent crosstalk and mutual coupling. The linear superposition of the resulting fields is represented by $L \times L$ block-diagonal matrix $\mathbf{S}^T = \mathrm{diag}\{\boldsymbol{\mu}^T, \ldots, \boldsymbol{\mu}^T\}$, where $1 \times K$ vector $\boldsymbol{\mu}^T = [1, 1, \ldots, 1]$.

2.1 Input-Output Relationship

Begin the analysis of Fig. 1 with the quantizer input,

$$\mathbf{u}(n) = (\mathbf{r} * \mathbf{a})(n) + (\mathbf{h} * \mathbf{e})(n) - \mathbf{e}(n),$$

where $*$ represents conventional discrete-time matrix-vector convolution. The quantizer output $\mathbf{w}(n) = \mathbf{u}(n) + \mathbf{e}(n)$ is then

$$\mathbf{w}(n) = (\mathbf{r} * \mathbf{a})(n) + (\mathbf{h} * \mathbf{e})(n).$$

Defining a temporal convolution in continuous/discrete-time by

$$(\mathbf{p} \star \mathbf{w})(\boldsymbol{x}, t) \triangleq T \sum_k \mathbf{p}(\boldsymbol{x}, t - kT)\, \mathbf{w}(k),$$

yields the output of the individual radiators, with T denoting both the system sampling interval and transpose^T. The combining of the element responses is represented by $\mathbf{S}^T$, so the total array current density output, before and after Fourier transforming on t, is

$$\begin{aligned} \mathbf{y}(\boldsymbol{x}, t) &= \big(\mathbf{S}^T\, \mathbf{p} \star \mathbf{r} * \mathbf{a}\big)(\boldsymbol{x}, t) \\ &\quad + \big(\mathbf{S}^T\, \mathbf{p} \star \mathbf{h} * \mathbf{e}\big)(\boldsymbol{x}, t) \end{aligned} \tag{1}$$

$$\begin{aligned} \mathbf{Y}(\boldsymbol{x}, f) &= \mathbf{S}^T \mathbf{P}(\boldsymbol{x}, f)\, T\mathbf{R}(fT)\, \mathbf{A}(fT) \\ &\quad + \mathbf{S}^T \mathbf{P}(\boldsymbol{x}, f)\, T\mathbf{H}(fT)\, \mathbf{E}(fT). \end{aligned} \tag{2}$$

On the right in each the first and second terms are the desired signal and the quantization error respectively, each shaped by the pulse matrix after filtering. To suppress the error term at spatio-temporal frequencies containing desired signal components, one must carefully choose the spatial locations of the antenna elements, the vector-quantization rule, the signal and noise frequency responses $\mathbf{R}(fT)$ and $\mathbf{H}(fT)$, and where possible the pulse-response matrix $\mathbf{p}(\boldsymbol{x}, t)$.

2.2 Far-Field Propagation

The spatial and temporal output of the array is given in (1) in terms of the current density $\mathbf{y}(\boldsymbol{x}, t)$. We are ultimately interested in the corresponding far-field array response, which can be found by solving Maxwell's equations. We use the method of [11], first solving for the vector potential $\mathbf{A}(\boldsymbol{x}, f)$, and then finding the electric field $\mathbf{E}(\boldsymbol{x}, f)$ in the far field. (These quantities are distinct from the previously defined $\mathbf{A}$ and $\mathbf{E}$, a notational abuse limited to this section.) The vector potential represents a spherical wave propagating away from each point on the antenna at a speed c:

$$\mathbf{A}(\boldsymbol{x}, f) = \frac{\mu}{4\pi} \int_{\mathcal{V}} \mathbf{Y}(\boldsymbol{x}', f) \frac{e^{-j2\pi \|\boldsymbol{x}' - \boldsymbol{x}\| f/c}}{\|\boldsymbol{x}' - \boldsymbol{x}\|}\, d\boldsymbol{x}', \tag{3}$$

where $\mathcal{V}$ is the spatial support of the current density $Y(\boldsymbol{x}, f)$. In the far field, defined here simply as $\|\boldsymbol{x}\| \to \infty$, the electric field can be found as

$$\mathbf{E}(\boldsymbol{x}, f) \approx -j2\pi f \mathbf{A}(\boldsymbol{x}, f) \tag{4}$$

for polarization components normal to the direction of propagation (the radial component vanishes). Combining (3) and (4), and letting direction vector $\boldsymbol{u} = \boldsymbol{x}/\|\boldsymbol{x}\|$ the far-field electric field can be reduced to

$$\mathbf{E}(\boldsymbol{x}, f) \approx \frac{-j\mu}{2\|\boldsymbol{x}\|} e^{-j2\pi \|\boldsymbol{x}\| f/c} f \int_{\mathcal{V}} \mathbf{Y}(\boldsymbol{x}', f) e^{j2\pi \boldsymbol{x}'^T \boldsymbol{u} f/c}\, d\boldsymbol{v}',$$

where we use the far-field approximation $\|\boldsymbol{x}' - \boldsymbol{x}\| \approx \|\boldsymbol{x}\|$ in the denominator (where the approximation is less critical) and the more precise approximation $\|\boldsymbol{x}' - \boldsymbol{x}\| \approx \|\boldsymbol{x}\| - \boldsymbol{x}'^T \boldsymbol{u}$ in the exponent. Recognizing a spatial Fourier transform and dividing out constants and factors dependent on the actual distance $\|\boldsymbol{x}\|$ yields the *normalized far-field* electric field

$$\frac{j2\|\boldsymbol{x}\|}{\mu} e^{j2\pi \|\boldsymbol{x}\| f/c} \mathbf{E}(\boldsymbol{x}, f) \approx f\, \hat{\mathbf{Y}}(-\boldsymbol{u} f/c, f). \tag{5}$$

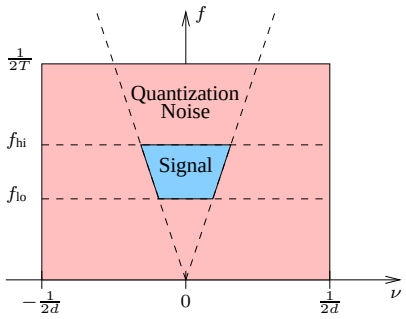

Figure 2: Spatio-temporal spectral regions.

Letting $\boldsymbol{v}$ denote spatial frequency, then, $\boldsymbol{v} = -\boldsymbol{u} f/c$ represents the frequencies corresponding to propagating radiation. Taking norms on both sides gives a version of the Helmholtz equation, $\|\boldsymbol{v}\| = f/c$. This defines the cone of propagating frequencies in $(\boldsymbol{v}, f)$ space. Spatial frequencies not on the cone do not propagate into the far field, and in this way the array acts as a particular ideal bandpass spatial filter. If we consider only a single spatial dimension, denoted by spatial variable z and corresponding spatial frequency v_z (appropriate for array elements on a line), then the projection of the cone into the (v_z, f) plane shown in Fig. 2 suggests how to choose the noise shaping in a space-time $\Delta\Sigma$ modulator. The center trapezoid represents the intersection of the temporal frequency band of interest and the cone, and represents the spectral support of the desired signal where quantization noise should be suppressed. The surrounding region then holds the shaped quantization errors. The rectangle represents the positive-frequency half of one period of the frequency response of the loop filter when the sampling rate is $1/T$ and the element spacing is d.

2.3 Array Pattern and Noise Transfer Function

We now examine in more detail the responses that modify signal and noise in (2). Writing the kth column of $\mathbf{S}^T \mathbf{P}(\boldsymbol{x}, f)$ as $\mathbf{P}_k(\boldsymbol{x} - \mathbf{x}_k, f)$ to indicate its spatial offset, the desired-signal (first) term of (2) becomes

$$\mathbf{Y}_s(\boldsymbol{x}, f) = \sum_n A_n(fT) \sum_k \mathbf{P}_k(\boldsymbol{x} - \mathbf{x}_k, f) T R_{k,n}(fT).$$

Transforming to the far-field yields

$$f\hat{\mathbf{Y}}_s(\boldsymbol{v}, f) = \sum_n A_n(fT) \sum_k f\hat{\mathbf{P}}_k(\boldsymbol{v}, f) T R_{k,n}(fT) e^{-j2\pi \mathbf{x}_k^T \boldsymbol{v}}. \tag{6}$$

The summation over k is the nth *array pattern*, the spatio-temporal transfer function applied to the nth input signal. If element responses are identical then $\hat{\mathbf{P}}_k(\boldsymbol{v}, f) = \hat{\mathbf{P}}_0(\boldsymbol{v}, f)$ can be factored from the summation over k, which is then recognized as a spatial Fourier transform:

$$f\hat{\mathbf{Y}}_s(\boldsymbol{v}, f) = f\hat{\mathbf{P}}_0(\boldsymbol{v}, f) T \sum_n \hat{R}_n(\boldsymbol{v}, fT) A_n(fT). \tag{7}$$

This extends the common separable array-pattern formulation to multiple inputs, with the pattern seen by nth input $A_n(fT)$ just the product of *element pattern* $f\hat{\mathbf{P}}_0(\boldsymbol{v}, f)$ and the nth *array factor* $T\hat{R}_n(\boldsymbol{v}, fT)$, which is the spatial and temporal Fourier transform of the nth column of $\mathbf{r}(n)$. Even though in a real design it is seldom sufficient to assume identical element patterns, this separable relationship between the element pattern and array factor is extremely convenient for analysis in the preliminary design stages. It also reinforces the the idea that far-field propagation effectively performs a spatial Fourier transform on the array output as a whole, as well as for each element.

Taking the error term of (2) through similar stages results in

$$f\hat{\mathbf{Y}}_e(\boldsymbol{v}, f) = \sum_n E_n(fT) \sum_k f\hat{\mathbf{P}}_k(\boldsymbol{v}, f) T H_{k,n}(fT) e^{-j2\pi \mathbf{x}_k^T \boldsymbol{v}} \tag{8}$$

for general element responses and

$$f\hat{\mathbf{Y}}_e(\boldsymbol{v}, f) = f\hat{\mathbf{P}}_0(\boldsymbol{v}, f) T \sum_n \hat{H}_n(\boldsymbol{v}, fT) E_n(fT) \tag{9}$$

for identical elements. Frequency response $\hat{H}_n(\boldsymbol{v}, fT)$ is the spatial and temporal shaping of element $E_n(fT)$ of the quantization error. We will revisit this expression in the next section when considering how to design $\mathbf{h}(n)$.

3. LOOP FILTER DESIGN

The performance of the array depend on two linear filters, the beamformer and the loop filter. Beamformer design has been considered many times in other contexts, but [12] specifically considers the case of close element spacing. The basic goal of the loop-filter design is to minimize the quantization error power in the spatio-temporal passband—that is, propagating spatial frequencies in the temporal frequency band of interest. Further, some constraints are required to maintain the stability and computability [13] of the modulator. The design is complicated somewhat by the fact that the loop filter, while time invariant, is not space invariant. Thus, there is not a single spatio-temporal transfer function to be optimized in the usual sense. However, under the common assumption that power spectral density $\mathbf{S}_e(fT) = \sigma^2\mathbf{I}$, so that the error vector is uncorrelated in both time and space, we can find the far-field in-band noise power in terms of the component error shaping transfer functions $\{\hat{H}_k(\boldsymbol{v}, fT)\}$. For simplicity we consider only a single polarization component, so $\mathbf{S} = [1, 1, \ldots, 1]^T$, and identical elements as before. Now the power in the combined array output is just the sum of the powers due to each element of the error vector, found by integrating the squared pattern over propagating frequencies and the signal band:

$$P_\epsilon = \sigma^2 \int_{\mathcal{F}} \int_{\Omega} |fT\hat{P}_0(\boldsymbol{v}, f)|^2 \sum_k |\hat{H}_k(\boldsymbol{v}, fT)|^2 \, dA(\boldsymbol{u}) \, df, \tag{10}$$

where $\mathcal{F}$ denotes the set of in-band temporal frequencies, Ω is the unit sphere, and dA is the surface-area measure. This expression is quadratic in the loop filter coefficients $\mathbf{h}(n)$ and can be minimized using a number of optimization techniques. If we assume no symmetry or other relationship between columns of $\mathbf{h}(n)$, then the K transfer functions $\{\hat{H}_k(\boldsymbol{v}, fT)\}$ are independently determined. Thus, to minimize the total power, we can independently optimize these transfer functions.

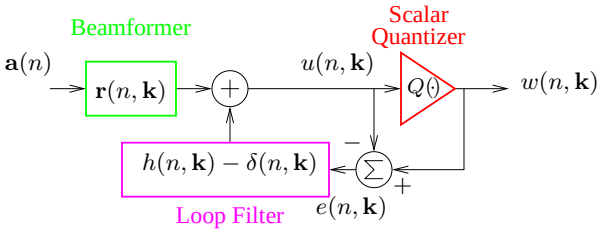

Figure 3: Shift-invariant multidimensional $\Delta\Sigma$ modulator.

When there is structure in the loop filter, such as limiting nonzero elements to a band around the main diagonal, we can further simplify the design process. Consider the following example unit-sample response for a small uniformly spaced linear array of five elements:

$$\mathbf{h}(n) = \begin{vmatrix} a_0(n) & b_{-1}(n) & 0 & 0 & 0 \\ a_1(n) & b_0(n) & c_{-1}(n) & 0 & 0 \\ 0 & b_1(n) & c_0(n) & d_{-1}(n) & 0 \\ 0 & 0 & c_1(n) & d_0(n) & e_{-1}(n) \\ 0 & 0 & 0 & d_1(n) & e_0(n) \end{vmatrix}$$

Structurally, the center three columns are related simply by a spatial shift. Since this shift has no effect on the power spectrum or total power, optimizing the corresponding transfer functions yields identical results. Thus $b_k(n) = c_k(n) = d_k(n)$, and the center portion of the optimized matrix impulse response is Toeplitz. For large arrays and impulse responses that are concentrated near the main diagonal, the difference between the optimal impulse response and a Toeplitz matrix formed by replicating and shifting one of the center columns becomes small. Not only does this simplify the design to that of a single column of $\mathbf{h}(n)$, but it has a convenient interpretation when compared to existing multidimensional $\Delta\Sigma$ modulator models for image halftoning [6] and sonar arrays [9]. These models assume a spatially shift-invariant structure such as that shown in Fig. 3, with a multidimensional (scalar) loop filter and a scalar quantizer. The implicit truncation required to keep input and output the same size actually renders the system shift variant, and this model only applies for uniform spatial support. It is straightforward to show that, when this system is converted to the equivalent vector $\Delta\Sigma$ structure, the resulting matrix loop filter is Toeplitz for a one-dimensional array. A similar result holds for two dimensional arrays, where the invariant impulse response becomes a block-Toeplitz matrix impulse response.

To constrain stability, one approach that has shown success in single-dimensional $\Delta\Sigma$ modulators [1, 14] is to limit the peak gain of the loop filter frequency response. Here, we can constrain the peak gain of the spatio-temporal transfer function $\hat{H}_k(\boldsymbol{v}, f)$ of each column of the loop filter for a space-varying design, or simply constrain the peak gain of the single transfer function in a space-invariant design. The best way to constrain stability is still an open question, and certainly other formulations exist that do not require a decomposition of the loop filter.

4. EXAMPLE

To illustrate, consider an example array with 101 identical elements spaced linearly with a uniform spacing. For a sampling rate of $f_s = 1/T_s$ we wish to transmit over a bandwidth of $f_s/8$ centered at $f_s/4$. The element spacing is $d = cT_s/2$, or half the wavelength at the sampling frequency. These parameters provide four-

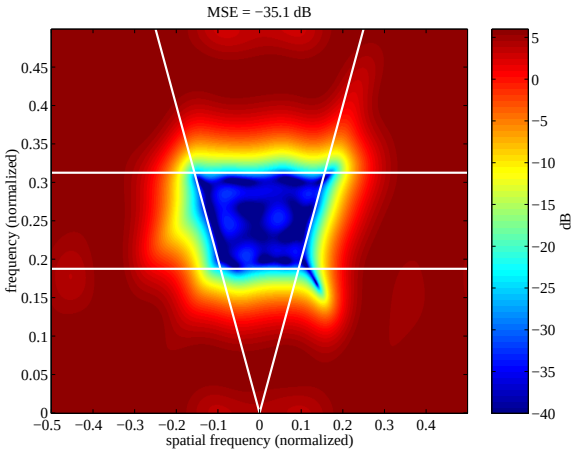

Figure 4: Optimized spatio-temporal frequency response applied to the error in a center element of the example array

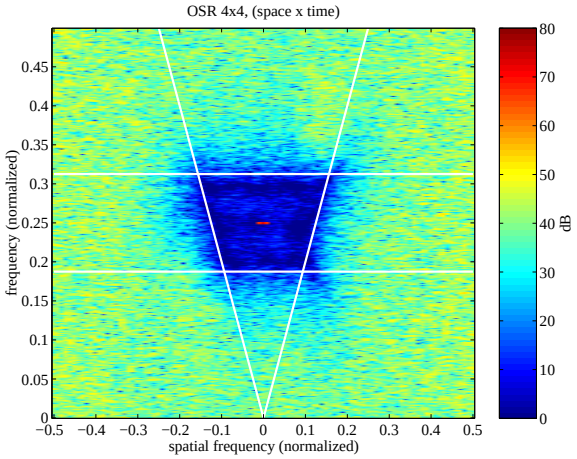

Figure 5: Simulated $\Delta\Sigma$-modulated signal spectrum for a narrowband, boresight beam using the filter of Fig. 4

times oversampling in both space and time. The loop filter is constrained to have scanning computability [13] and is 11 taps long in time. In space the filter is 11 elements wide, symmetrically spaced. Since this is much smaller than the array width a Toeplitz structure will be used, and only one of the center responses $\hat{H}_k(\boldsymbol{v}, f)$ needs to be optimized, minimizing the mean-square signal-band gain while restricting the gain elsewhere to 6 dB to preserve modulator stability. Fig. 4 shows the positive-frequency half of one period of the resulting magnitude response, where the propagating cone (spatial bandwidth) and signal bandwidth are indicated by the diagonal and horizontal lines, respectively. Fig. 5 shows the resulting output spectrum $\hat{R}(\boldsymbol{v}, fT)A(fT) + \sum_n \hat{H}_n(\boldsymbol{v}, fT)E_n(fT)$ prior to the radiating elements with a single hamming-weighted sinusoidal input $a(n)$ and hamming-weight beamformer $\mathbf{r}(n)$. The close resemblance between the shaped noise spectrum and Fig. 4 serves to justify the Toeplitz and white-noise assumptions.

5. CONCLUSIONS

In this paper we have described a new digital transmit array architecture incorporating space-time vector $\Delta\Sigma$ modulation for high linearity. Far-field wave propagation was shown to act like an ideal bandpass filter to remove the resulting shaped quantization errors. This architecture is more general than existing multidimensional $\Delta\Sigma$ architectures as it makes no assumptions of regular spatial sampling or spatial shift invariance. However, under common conditions we show that the optimal shift-invariant (Toeplitz) loop filter is a good approximation of the general solution.

REFERENCES

[1] J. C. Candy and G. C. Temes, "Oversampling methods for A/D and D/A conversion," in *Oversampled Delta-Sigma Data Converters*. IEEE Press, New York, 1991.

[2] R. Schreier and B. Zhang, "Noise-shaped multibit D/A converter employing unit elements," *Electronics Letters*, vol. 31, no. 20, pp. 1712–1713, Sept. 1995.

[3] I. Galton, "Spectral shaping of circuit errors in digital-to-analog converters," *IEEE Trans. Circuits and Systems II*, vol. 44, no. 10, pp. 808–817, Oct. 1997.

[4] D. P. Scholnik and J. O. Coleman, "Joint shaping of quantization and hardware-mismatch errors in a multibit delta-sigma DAC," in *Proc. 2000 Midwest Symp. on Circuits and Systems (MWSCAS 2000)*, Lansing MI, Aug. 2000.

[5] R. Floyd and L. Steinberg, "An adaptive algorithm for spatial grayscale," *Proc. Soc. Image Display*, vol. 17, no. 2, pp. 75–77, 1976.

[6] T. D. Kite, B. L. Evans, A. C. Bovik, and T. L. Sculley, "Digital halftoning as 2-D delta-sigma modulation," in *Proc. IEEE Int. Conf. Image Processing*, 1997, pp. 799–802.

[7] D. P. Scholnik and J. O. Coleman, "Joint spatial and temporal delta-sigma modulation for wideband antenna arrays and video halftoning," in *Proc. IEEE Int. Conf. Acoustic, Speech, and Signal Processing*, Salt Lake City, UT, May 2001.

[8] M. Iwamoto, A. Jayaraman, G. Hanington, P. Chen, A. Bellora, W. Thornton, L. Larson, and P. Asbeck, "Bandpass delta-sigma class-S amplifier," *Electronics Letters*, vol. 36, no. 12, pp. 1010–1012, June 2000.

[9] Y. Tamura, N. Kawakami, O. Akasaka, M. Okada, and K. Koyama, "Beam-forming using multidimensional sigma-delta modulation," in *Proc. IEEE Ultrasonics Symp.*, 1998, pp. 1077–1080.

[10] D. P. Scholnik and J. O. Coleman, "Vector delta-sigma modulation with integral shaping of hardware-mismatch errors," in *IEEE 2000 Int'l Symp. on Circuits and Systems (ISCAS 2000)*, Geneva, Switzerland, May 2000.

[11] C. A. Balanis, *Antenna Theory*, John Wiley & Sons, Inc., 1982.

[12] D. P. Scholnik and J. O. Coleman, "Superdirectivity and SNR constraints in wideband array-pattern design," in *IEEE Int'l Radar Conference*, Atlanta, GA, May 2001.

[13] D. P. Scholnik and J. O. Coleman, "Computability constraints in space-time delta-sigma arrays," in *Proc. Asilomar Conf. on Signals, Systems, and Computers*, Pacific Grove, CA, Nov. 2001.

[14] *Delta-Sigma Data Converters : Theory, Design, and Simulation*, IEEE Press, New York, 1996.